International Journal of Engineering Science 47 (2009) 537–553

Contents lists available at ScienceDirect

International Journal of Engineering Science

journal homepage: www.elsevier.com/locate/ijengsci

A revisited generalized self-consistent polycrystal model following an incremental small strain formulation and including grain-size distribution effect

S. Ramtani *, H.Q. Bui, G. Dirras

Laboratoire des Propriétés Mécaniques et Thermodynamiques des Matériaux – LPMTM, CNRS UPR 9001, Université Paris 13, 99 Avenue J.B. Clément, 93430 Villetaneuse, France

ARTICLE INFO

Article history:
Received 8 May 2008
Received in revised form 16 June 2008
Accepted 10 September 2008
Available online 12 November 2008

Keywords:
Micromechanics
Nanocrystalline materials
Grain-size effect
Numerical simulation

ABSTRACT

A generalized self-consistent approach, recently proposed by Jiang and Weng (2004) [B. Jiang, G.J. Weng, A generalized self-consistent polycrystal model for the yield strength of Nanocrystalline materials, Journal of the Mechanics and Physics of Solids 52 (2004a) 1125–1149; B. Jiang, G.J. Weng, A theory of compressive yield strength of nano-grained ceramics, International Journal of Plasticity 20 (2004b) 2007-2056.] for investigating the so-called "breakdown" of the Hall–Petch law in the case of nanocrystalline (NC) materials, is revisited and reformulated following an incremental small strain scheme. The NC material is modelled as a composite material that takes each oriented grain and its immediate grain boundary to form a pair, which in turn is embedded in the infinite effective medium with a property representing the average orientation of all these pairs. The plastic deformation of the inclusion phase takes into account the dislocation glide mechanism whereas boundary phase is modelled as an amorphous material. As an application, the model's parameters are identified under an optimization code with respect to data stated from pure copper submitted to tensile load. The aggregate is composed of spherical randomly distributed grains with a grain-size distribution following a log-normal statistical function.

1. Introduction

As an enormous industry, powder metallurgy deals currently with the production of sophisticated metal that exhibit extremely attractive and useful properties of high density, hardness, fracture toughness, surface activity, dispersibility, safety and endurance to heat. Such properties can be exploited for a variety of structural and non-structural applications. Requirement for ultra fine microstructures produced by powder metallurgy persists to grow for new applications such as Catalysts and Hydrogen Storage, Conducting Paste, and Solid Rocket Fuel. These applications are identified and developed with respect to many advantages such as increased surface area, increased electrical conductivity, enhanced magnetic properties, size dependant absorption properties and faster sintering kinetics.

Bulk ultra fine-grained metals are those having grains diameter of submicron order, but generally greater than 100 nm. They have exceptional mechanical properties like high strength with, in many cases, reasonable ductility and a great ability to save production costs. They are often produced by one of two well-know methods such as, severe plastic deformation (SPD) of conventional grain-size materials, and powder metallurgy-based methods (PM) [1–4]. In the mid-1980s, Gleiter [5] made the visionary argument that metals and alloys, if made NC, (average grain size <100 nm) would have a number

* Corresponding author. Tel.: +33 149403953; fax: +33 149403938.
E-mail address: ramtani@galilee.univ-paris13.fr (S. Ramtani).

0020-7225/$ - see front matter © 2008 Elsevier Ltd. All rights reserved.
doi:10.1016/j.ijengsci.2008.09.005

of appealing mechanical characteristics of potential significance for structural applications. They are thus of considerable interest from both scientific and technological viewpoints [6–9].

The properties of NC metals have been a major focus for computational materials science in recent years, particularly the behaviour of the grain boundaries (GBs) with their underlying structure which are known to play an important role, and often associated with the atomic level mechanisms of plastic deformation, as analyzed through experiments [10–13], atomistic simulations [14–18] and theoretical models [19–24]. Many researchers have treated NC materials as composite materials with a grain interior phase and inter-grain phase (sometimes including grain boundary, triple line, and quadruple node), and have adopted different models for the phases, after evaluating their respective volume fractions, to describe the overall mechanical behaviour. These methods include the rule of mixture-based models [25–28], the generalized self-consistent models which incorporated the plastic anisotropy of the grains, their orientations, and the stress heterogeneity of the grains and the grain-boundary phase [22,23], the homogenization method [29] to describe the grain size and strain rate effect on the stress–strain relations, the aggregate deformation gradient model [30] and finite element (FE) methods [31–34].

One can note that the difficulty in predicting grain-size effects arises from the differences in physical processes occurring within the grain-boundary region and grain interiors [33–35]. More precisely, additional intergranular accommodation mechanisms such as grain-boundary slip, cavitation, and microcracking, must be operative. Experimental evidence of such mechanisms may be found in Ref. [36]. In a recent paper, Wei and Anand [33] formulated a rate-independent constitutive model of a cohesive interface that accounts for reversible elastic and irreversible inelastic slip – separation deformations at a grain boundary prior to failure. Further, atomistic simulations also show void formation and decohesion leading to intergranular fracture in NC materials [37,38].

A first micro–macro modelling considering grain-size effect has been elaborated by Weng [39] who considered a Hall–Petch type equation with a single valued grain size at the scale of the slip systems and used the Berveiller–Zaoui's model [40] to derive the overall behaviour of copper polycrystals which lead to a Hall–Petch type behaviour as well. More recently, non-local dislocation mechanics models using the concept of geometrically necessary dislocations (GNDs) have been developed by Acharya and Beaudoin [41] and predict well the strain-hardening rate dependence on grain size after the yield point making use of the evolution of GNDs (or equivalently the lattice incompatibility). Contrarily to recent works [42–45], in these developments only the mean grain size is considered, and most of the advanced homogenization techniques developed these last decades such as the self-consistent procedure did not focused on the effect of grain-size distribution and did not account for statistical description which are stochastic internal parameters of the heterogeneous microstructure. Since the grain size distribution provides heterogeneity, it appears fundamental to get an accurate description of the effect of grain size on the local interactions and behaviours, and also, a relevant mathematical description of the grain-size statistics inherent to the processing route. Taking advantage of recent works [43–45], the objective of the present paper is to investigate grain-size effects on the mechanical behaviours of heterogeneous NC materials assuming a given grain-size distribution with respect to the role of the grain-size dispersion.

2. Model formulation

Even if recent molecular dynamics simulations (MD) of NC materials have motivated the particular micro-geometry including two distinct regions of the material (i.e., the interconnected grain-boundary phase and the isolated grains of various orientations), a number of existing models treat the composite as a two-phase material with a perfect interface [22,23,29,42,46]. Because this is a strong idealization and sometimes not consistent with experimental observations, Jiang and Weng [22,23] have derived a generalized self-consistent model which offers some capabilities such as plastic anisotropy of the grains, their orientations, and the stress heterogeneity of the grains and grain-boundary phase. The interested reader can find more details and arguments in the reference paper [22,23] that have inspired this research work and from which an incremental small strain formulation of the generalized self-consistent polycrystalline model is stated.

2.1. Constitutive equations of the grain phase

The overall small strain elastoplastic response of the NC polycrystal will be calculated by the approach of a linear comparison composite [22,23,47–52]. Thus, the linear auxiliary problem is one that involves the superposition of Christensen and Lo's [53] two-phase generalized self-consistent scheme and Luo and Weng's [54] three-phase concentrated eigenstrain problem. Such a superposition is schematically shown in Fig. 1 and taken back from [22,23]. Both solutions were given for elastically isotropic constituents, and thus for simplicity the crystallites will also be taken to be elastically isotropic while retaining its plastic anisotropy. From the local stress field of their solutions, one can take the volume average to find the mean stresses of the grain of a given orientation, and grain-boundary phase.

Under both small strain assumption and initially stress free at macroscopic level, the applied stress rate $\dot{\boldsymbol{\Sigma}}$ and strain rate $\dot{\mathbf{E}}$ are linearly related through the macroscopic tangent elastoplastic stiffness $\mathbf{L}^{\mathbf{c}}$

$$\dot{\Sigma}_{ij} = L^{c}_{ijkl}\dot{E}_{kl}. \tag{1}$$

In accordance with the slip model of crystal plasticity, the mean plastic strain rate of the grain is given by

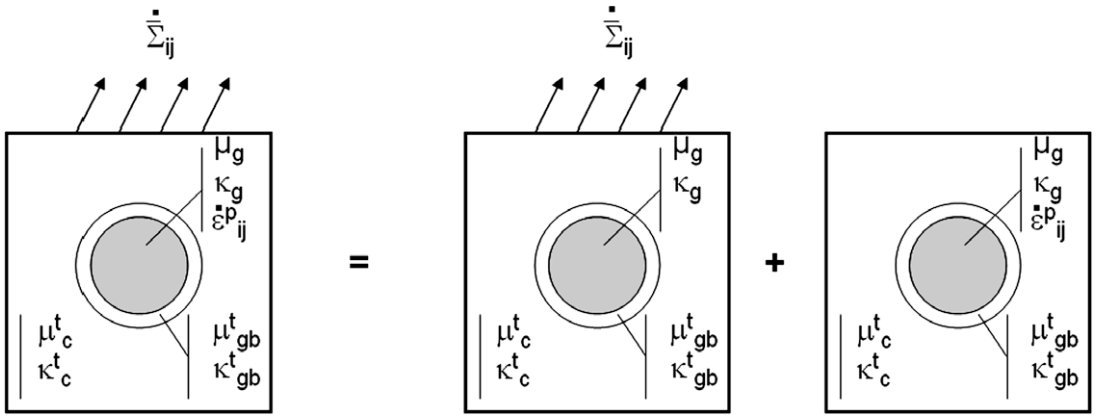

Fig. 1. Superposition of two linear problems.

$$\dot{\bar{\varepsilon}}^{p(g)}_{ij} = \sum_{s=1}^{N} \frac{1}{2}\left(n_i^{(s)} b_j^{(s)} + n_j^{(s)} b_i^{(s)}\right)\dot{\gamma}^{(s)} = \sum_{s=1}^{N} p_{ij}^{(s)} \dot{\gamma}^{(s)}, \tag{2}$$

where $b_i^{(s)}$ is a unit vector in the slip direction of the sth slip system on the slip plane with unit normal $n_i^{(s)}$, $\dot{\gamma}^{(s)}$ is the corresponding slip rate, and the definition of $p_{ij}^{(s)}$ is clear from the context. The rate of change of resistance to slip is governed by the microscopic hardening rule

$$\dot{\tau}^{(s)} = \sum_{s'=1}^{N} h^{(ss')} \dot{\gamma}^{(s')}, \tag{3}$$

where s and s' run over all the slip systems, $h^{(ss')}$ is the hardening matrix and $\dot{\tau}^{(s)}$ is the rate of change of the resolved shear stress $\tau^{(s)} = p_{ij}^{(s)} \bar{\sigma}_{ij}^{(g)}$ (no sum on s); $\dot{\gamma}^{(s)}$ is nonzero if Eq. (3) is satisfied and $p_{ij}^{(s)} \bar{\sigma}_{ij}^{(g)} = \tau_y^{(s)}$, where $\tau_y^{(s)}$ is the current yield stress in shear for the sth slip system.

With analyzing experimental Hall–Petch data of many of materials, the description of three regions is widely adopted: (1) a region from single crystal to a micrometer grain size where the classical Hall–Petch description can be successfully used; (2) a region for grain sizes ranging from 1 μm to 30 nm where the Hall–Petch relation roughly holds, but deviates from the classical power −0.5 to the value near to zero; (3) a region beyond a very small critical grain size where the Hall–Petch slope is nearly zero with no increase in strength with grain size decreasing. On the basis of the dislocation pile-up mechanism for the plastic deformation of coarse-grained materials, the empirical Hall–Petch relation which suggests that the yield stress increases with the decreasing of the grain size has been stated as [55,56]

$$\tau_y^{(s)} = \tau_\infty^{(s)} + \frac{k}{\sqrt{d}}, \tag{4}$$

where $\tau_\infty^{(s)}$ is the friction stress (identical for the whole grains) and k is the slope of the grain-size dependent relationship. In the present formulation, both materials parameters are assumed strain independent. The components of the hardening matrix is chosen as

$$h_{ij} = \left(h_\gamma + \frac{a}{\sqrt{d}}\right)\left(q + (1-q)\delta_{ij}\right), \tag{5}$$

where δ_{ij} is Kronecker's delta and the subscript ∞ signifies the value of a grain with an infinite grain size (i.e. free crystal), and k and a are material constants. The factor q determines the degree of latent hardening, e.g. $q = 0$ provides only self hardening, $q = 1$ provides Taylor's hardening and $q > 1$provides stronger latent hardening than self hardening.

It is also assumed that the instantaneous hardening coefficient h_γ depends on the previous deformation history. In the present model, the relation between the accumulated slip in the grain, γ^{acc}, and the instantaneous hardening coefficient is described by an exponentially decreasing function [57]:

$$h_\gamma = h_{\text{final}}\left(1 + (h_{\text{ratio}} - 1)\mathrm{e}^{-h_{\exp}\gamma^{acc}}\right), \tag{6}$$

where h_{final} is the final hardening coefficient, h_{ratio} is the ratio between the initial and the final hardening coefficient, and $h_{\exp}$ is a parameter determining the strength of the exponential part. This formulation of the hardening law includes the simple linear hardening, that is obtained by choosing $h_{\text{ratio}} = 1$.

The stress rate in the grain, which is assumed initially stress free, (crystal) is given in terms of the crystal elasticity tensor $C^{(g)}$ and elastic strain rate

$$\dot{\sigma}_{ij}^{(g)} = C_{ijkl}^{(g)}\left(\dot{\varepsilon}_{kl}^{(g)} - \sum_{s} p_{kl}^{(s)}\dot{\gamma}^{(s)}\right), \tag{7}$$

where $\dot{\sigma}_{ij}^{(g)}$ are the components of the Cauchy stress rate tensor and $\dot{\varepsilon}_{kl}^{(g)}$ are the components of the total strain rate of the grain.

In what follows, any fourth order tensor $\overline{Z}_{ijkl}$ (respectively $\bar{\alpha}, \bar{\beta}$) is deduced from Christensen and Lo's [53] elastic solution whereas $\tilde{z}_{ijkl}$ (Respectively $\tilde{\alpha}, \tilde{\beta}$) is deduced from Luo and Weng's [54] three-phase concentrated eigenstrain problem solution. Following previous work [23,24], one can note that the total granular strain rate $\dot{\varepsilon}_{ij}^{(g)}$ can be cast as follows

$$\dot{\varepsilon}_{ij}^{(g)} = \overline{M}_{ijkl}^{(g)}\dot{\Sigma}_{kl} + \tilde{\ell}_{ijkl}^{(g)}\dot{\varepsilon}_{kl}^{p(g)}, \tag{8}$$

where the first term correspond to Christensen and Lo's [53] elastic solution whereas the second correspond to the Luo and Weng's [54] three-phase concentrated eigenstrain problem solution. The local tensors $\overline{M}_{ijkl}^{(g)}, \tilde{\ell}_{ijkl}^{(g)}$ are as follows

$$\left|\begin{array}{l} \overline{M}_{ijkl}^{(g)} = \frac{\bar{\beta}_g}{2\mu_g}\delta_{ijkl} + \frac{1}{3}\left(\frac{\bar{\alpha}_g}{3\kappa_g} - \frac{\bar{\beta}_g}{2\kappa_g}\right)\delta_{ij}\delta_{kl} \\ \tilde{\ell}_{ijkl}^{(g)} = \tilde{\beta}_g\delta_{ijkl} + \frac{1}{3}(\tilde{\alpha}_g - \tilde{\beta}_g)\delta_{ij}\delta_{kl} \end{array}\right. \tag{9}$$

and the parameters $\bar{\alpha}_g, \bar{\beta}_g, \tilde{\alpha}_g, \tilde{\beta}_g$ have been previously stated by (Jiang and Weng [22,23]) and reported in the Appendix with respect to tangent elastic modulus instead of secant one.

Projecting both sides of Eq. (7) on the Schmid tensor and using Eqs. (2), (3) and (8) the following relation is derived [40,58,59]

$$\sum_{s'}\left\{h^{(ss')} - p_{ij}^{(s)}C_{ijkl}^{(g)}\left(\tilde{\ell}_{klpq}^{(g)} - \delta_{klpq}\right)p_{pq}^{(s')}\right\}\dot{\gamma}^{(s')} = p_{ij}^{(s)}C_{ijkl}^{(g)}\overline{M}_{klpq}^{(g)}\dot{\Sigma}_{pq}. \tag{10}$$

If for given set of S active systems, it is possible to invert the S x S matrix $\boldsymbol{X}$ defined as

$$X^{ss'} = h^{(ss')} - p_{ij}^{(s)}C_{ijkl}^{(g)}\left(\tilde{\ell}_{klpq}^{(g)} - \delta_{klpq}\right)p_{pq}^{(s')} \tag{11}$$

then the following relation holds

$$\dot{\gamma}^{(s)} = Q_{pq}^{(s)}\dot{\Sigma}_{pq}, \tag{12}$$

where second rank tensor $Q_{pq}^{(s)}$ associated with each active system s is comparable to the one given by [40,58,59]

$$Q_{pq}^{(s)} = \sum_{s'}(X^{ss'})^{-1}p_{ij}^{(s')}C_{ijkl}^{(g)}\overline{M}_{klpq}^{(g)}. \tag{13}$$

With the aid of Eq. (12) and under the simultaneous influence of an external stress and eigenstrain, the total mean stresses in the grain of a given orientation are the sum of the two,

$$\dot{\sigma}_{ij}^{(g)} = \left(\overline{B}_{ijkl}^{(g)} + \tilde{b}_{ijkl}^{(g)}\right)\dot{\Sigma}_{kl}, \tag{14}$$

where the stress concentration tensors are specialized as

$$\left|\begin{array}{l} \overline{B}_{ijkl}^{(g)} = \frac{(\bar{\alpha}_g - \bar{\beta}_g)}{3}\delta_{ij}\delta_{kl} + \bar{\beta}_g\delta_{ijkl} \\ \tilde{b}_{ijkl}^{(g)} = \xi\left\{2\mu_g\left(\tilde{\beta}_g - 1\right)\delta_{ijkl} + \left[\kappa_g\left(\tilde{\alpha}_g - 1\right) - \frac{2\mu_g\left(\tilde{\beta}_g - 1\right)}{3}\right]\delta_{ij}\delta_{kl}\right\} \\ \xi = \sum_{s=1}^{N} p_{pq}^{(s)}Q_{pq}^{(s)}. \end{array}\right. \tag{15}$$

For a given orientation, the microscopic and macroscopic strain rate can be related through the localization tensor $A_{ijkl}^{(gb)}$

$$\dot{\varepsilon}_{ij}^{(g)} = \left\{\overline{M}_{ijrs}^{(g)} + \tilde{m}_{ijrs}^{(g)}\right\}L_{rskl}^{c}\dot{E}_{kl} = A_{ijkl}^{(g)}\dot{E}_{kl}, \tag{16}$$

where $\tilde{m}_{ijkl}^{(g)} = \xi\left\{\tilde{\beta}_g\delta_{ijkl} + \frac{1}{3}\left(\tilde{\alpha}_g - \tilde{\beta}_g\right)\delta_{ij}\delta_{kl}\right\}$.

2.2. Constitutive equations of the grain-boundary phase

To describe such a plastic behaviour for the amorphous, initially stress free, grain-boundary phase by a continuum model, we invoke Drucker's [60] constitutive equation, which has also proven suitable for the modeling of metallic glasses [61]. Drucker's equation not marked here by the pressure dependence of the yield stress; can be written as [22,23]

$$\sigma_e^{(gb)} = \sigma_Y^{(gb)} + h^{(gb)}(\varepsilon_e^{p(gb)})^{n_{gb}}, \tag{17}$$

where $\sigma_e^{(gb)} = \sqrt{\left(\frac{3}{2}\overline{S}_{ij}^{(gb)}\overline{S}_{ij}^{(gb)}\right)}$ is the Von Mises equivalent stress, $\overline{S}_{ij}^{(gb)} = \bar{\sigma}_{ij}^{(gb)} - \frac{\bar{\sigma}_{kk}^{(gb)}}{3}\delta_{ij}$ is the stress deviator tensor, $\sigma_Y^{(gb)}$ is the Von Mises yield stress, $h^{(gb)}$ is the strength coefficient, n_{gb} is the work-hardening exponent and $\varepsilon_e^{p(gb)} = \int\sqrt{\frac{2}{3}\dot{\varepsilon}_{ij}^{p\prime(gb)}\dot{\varepsilon}_{ij}^{p\prime(gb)}}\mathrm{d}t$ is the effective plastic strain.

For the application of the linear comparison composite with a tangent-modulus formulation, the tangent Youngs modulus, the tangent Poisson ratio, the tangent bulk and the shear modulus are re-written as [22,23]

$$\left|\begin{array}{l} E_{(gb)}^t = \left(\frac{1}{E_{(gb)}} + \frac{d\varepsilon_e^{p(gb)}}{d\sigma_e^{(gb)}}\right)^{-1}, \quad \nu_{(gb)}^t = \frac{1}{2} - \left(\frac{1}{2} - \nu_{(gb)}\right)\frac{E_{(gb)}^t}{E_{(gb)}} \\ \kappa_{(gb)}^t = \left(\frac{E_{(gb)}^t}{3(1-2\nu_{(gb)}^t)}\right), \quad \mu_{(gb)}^t = \left(\frac{E_{(gb)}^t}{2\left(1+\nu_{(gb)}^t\right)}\right). \end{array}\right. \tag{18}$$

With the aid of Eq. (12) and under the simultaneous influence of an external stress and eigenstrain, the total mean stresses in the surrounding grain boundary are the sum of the two

$$\dot{\bar{\sigma}}_{ij}^{(gb)} = (\overline{B}_{ijkl}^{(gb)} + \tilde{b}_{ijkl}^{(gb)})\dot{\Sigma}_{kl}, \tag{19}$$

where the stress concentration tensors are specialized as

$$\left|\begin{array}{l} \overline{B}_{ijkl}^{(gb)} = \bar{\beta}_{gb}\delta_{ijkl} + \frac{(\bar{\alpha}_{gb} - \bar{\beta}_{gb})}{3}\delta_{ij}\delta_{kl} \\ \tilde{b}_{ijkl}^{(gb)} = \xi\left\{2\mu_{gb}^t\tilde{\beta}_{gb}\delta_{ijkl} + \left[\kappa_{gb}^t\tilde{\alpha}_{gb} - \frac{2\mu_{gb}^t\tilde{\beta}_{gb}}{3}\right]\delta_{ij}\delta_{kl}\right\}. \end{array}\right. \tag{20}$$

For a given orientation, the microscopic and macroscopic strain rate can be related through the localization tensor $A_{ijkl}^{(gb)}$

$$\dot{\bar{\varepsilon}}_{ij}^{(gb)} = \left\{\overline{M}_{ijrs}^{(gb)} + \tilde{m}_{ijrs}^{(gb)}\right\}L_{rskl}^c\dot{E}_{kl} = A_{ijkl}^{(gb)}\dot{E}_{kl} \tag{21}$$

$$\left|\begin{array}{l} \overline{M}_{ijkl}^{(gb)} = \frac{\bar{\beta}_{gb}}{2\mu_{gb}^t}\delta_{ijkl} + \frac{1}{3}\left(\frac{\bar{\alpha}_{gb}}{3\kappa_{gb}^t} - \frac{\bar{\beta}_{gb}}{2\kappa_{gb}^t}\right)\delta_{ij}\delta_{kl} \\ \tilde{m}_{ijkl}^{(gb)} = \xi\left\{\tilde{\beta}_{gb}\delta_{ijkl} + \frac{1}{3}\left(\tilde{\alpha}_{gb} - \tilde{\beta}_{gb}\right)\delta_{ij}\delta_{kl}\right\}. \end{array}\right. \tag{22}$$

On the topological point of view, the RVE is composed of spherical grains and we also assume that grain size is spatially non-correlated, which means that the spatial position of grains of a given diameter is truly random. Hence, in terms of the grain size (diameter) d and grain-boundary thickness δ, the volume fraction of the grains can be approximated by $cg = \left(\frac{d}{d+\delta}\right)^3$.

The overall strains of the Nanocrystalline material under a given level of external stress then follow from the orientational average over all grain orientations and their respective grain boundaries. Then, local and macroscopic magnitudes are linked through the following micro–macro relations

$$c_g\left\langle\dot{\bar{\varepsilon}}_{ij}^{(g)}(\varphi_1,\phi,\varphi_2)\right\rangle + (1-c_g)\left\langle\dot{\bar{\varepsilon}}_{ij}^{(gb)}(\varphi_1,\phi,\varphi_2)\right\rangle = \dot{E}_{ij} \tag{23}$$

$$c_g\left\langle\dot{\bar{\sigma}}_{ij}^{(g)}(\varphi_1,\phi,\varphi_2)\right\rangle + (1-c_g)\left\langle\dot{\bar{\sigma}}_{ij}^{(gb)}(\varphi_1,\phi,\varphi_2)\right\rangle = \dot{\Sigma}_{ij}, \tag{24}$$

where $\langle\cdot\rangle$ denotes the volume average, $(\varphi_1,\phi,\varphi_2)$ represent the Euler angles of the rotation (or orientation) of a grain with respect to a base lattice (say a cubic lattice) that are aligned along the external loading coordinates, as indicated in the reference paper [22,23].

2.3. Grain-size distribution function

Despite the fact that the grain-size distribution in heterogeneous materials provides heterogeneity that can be characterized by methods such as transmission electron microscopy (TEM) and X-ray diffraction, most of the published works considers the mean grain size as the adequate parameters to describe the structure of the sample material. Therefore, it appears fundamental to get an accurate description of the effect of grain size on the local interactions and behaviours, and also, a relevant mathematical description of the grain-size statistics inherent to the processing route [43–45,62].

The dispersion of the grain size is presented by the lognormal distribution function [43–45]

$$p(D) = \frac{1}{\sqrt{2\pi}D\cdot S}\exp\left[-\frac{1}{2}\left(\frac{\ln(D)-M}{S}\right)^2\right], \tag{25}$$

where $\int_0^\infty p(D)\mathrm{d}D = 1$, D is the diameter of the grain, M and S are constant parameters describing the mean grain size and standard deviation of the lognormal distribution. When considering mechanical behaviour, the volume fraction of individual grain-size classes is of primary importance. Using the frequency distribution, i.e. here the log-normal distribution, $p(D)$, volume fraction of grains with size D, $p_v(D)$, can be written as [45,63]:

$$p_v(D) = \frac{kD^3}{V} p(D), \tag{26}$$

where the total volume of the sample is $V = \int_0^\infty kD^3 p(D)\mathrm{d}D$, k is a constant describing the shape of the grains (e.g., $k = \frac{4}{3}\pi\frac{1}{2^3}$ for a sphere).

The procedure to generate different discrete log-normal distributions with given means and dispersions follows procedure adopted by previous works [43–45]. For example, Fig. 2 displays the plot of statistical volume weighted distributions for various relative dispersions assuming a mean grain diameter of 110 nm.

3. Application to NC copper

3.1. Grain-size distribution function

As in the original work of Jiang and Weng [22,23] tensile data of Sanders et al. [2,64] have been considered for comparison with the revisited theory to evaluate the stress–strain relation and yield strength of copper during the micro-to-nano grain transition. The tensile tests covered four mean grain sizes but here only three of them are used here: 20 μm, 110 nm and 49 nm; and the corresponding stress–strain curves have been reported in Fig. 3 and compared to the current model prediction with respect to the set of parameters given in the Table 1. These parameters have been identified via an optimization code (SiDoLo) that is based on an inverse analysis approach, and which consists of minimizing the function representing the difference between the experimental data and the data obtained by integrating the model [65,66]. In our calculations, the total number of grains (or grain orientations) was 400, generated through random rotations of the Euler angles $(\varphi_1,\phi,\varphi_2)$. Following the suggestion of Chokshi et al. [67] for copper and the previous contribution of Jiang and Weng [22,23], the grain-boundary thickness was taken to be $\delta = 1$ nm. Atomic simulations have indicated that the grain boundary thickness has little correlation with the grain size [68] (Table 2).

In order to uncover the transition of yield strength in light of the Hall–Petch relation, the yield stresses at 0.2% plastic strain are plotted in Fig. 4 as a function of $(D_{\mathrm{mean}})^{-1/2}$. The "relative" dispersion $\Delta D/D$ which differs from 0 takes the respective values 1, 2, 4 and 6 and all the curves appear to be quite linear (Fig. 4). Our results, like those presented by Berbenni et al [43,44], display a unique effect of the grain-size dispersion which becomes more significant at finest mean grain sizes in nano range (here 49 nm). One can note that this effect, i.e., the "relative" dispersion, had also been found by Kurzydlowski [69] which presented its results in terms of Standard deviations using however crude assumptions like Uniform plastic strain or plastic strain within a grain proportional to its volume, and, computing the flow stress using a simple averaging rule of mixture on the distributed grains volume.

3.2. Local plastic strain fields

The present micromechanical model has the capability to record the evolutions of plastic strain and internal stresses within grains (*g*) and grain-boundaries (*gb*) which are non-uniform when grains have different sizes. In what follows: (1) for all figures, results for the grains are reported on left parts and the ones for the grain-boundary are reported on right parts, (2) both plastic strain and local stress distributions are shown for the two phases, and investigated for slight relative dispersion $\Delta D/D = 1$ and broad relative dispersion $\Delta D/D = 6$ around the mean grain sizes of 20 μm, 110 nm and 49 nm.

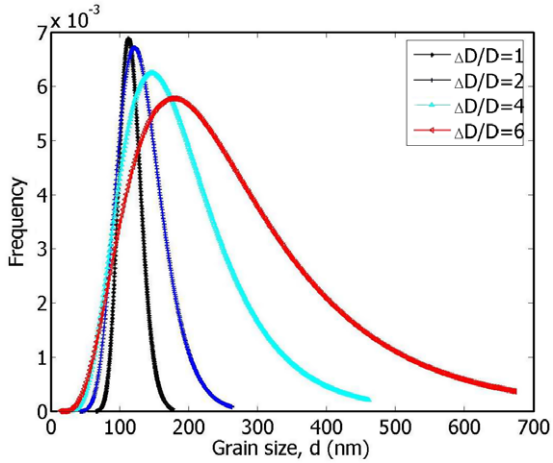

Fig. 2. Volume weighted grain-size distribution calculated with the mean grain size of 110 nm and various relative dispersions.

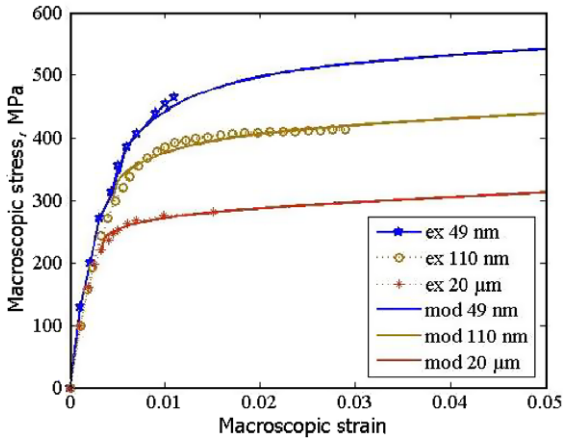

Fig. 3. Calculated and experimental stress–strain relations of nanocrystalline copper during the coarse to nano-grain transition.

Evolutions of local plastic strains (component $\bar{\varepsilon}_{33}^{p(g)}$ and $\bar{\varepsilon}_{33}^{p(gb)}$ in the axial loading direction 3) are reported on Figs. 5–10 at three stages of macroscopic plastic strains E_{33}^{p}: 0.2%, 1% and 2%. Regarding coarsest grains with D_{mean}= 20 µm (Figs. 5 and 6), local plastic strains are homogeneous, higher in the grains (Figs. 5 and 6a) than in the grain-boundaries (Figs. 5 and 6b). As expected, one can note that the relative dispersion do not disturb the local plastic strains distribution.

Regarding now the intermediate mean grain size D_{mean} = 110 nm, it is found that for $\Delta D/D = 1$ (Fig. 7a,b), local plastic strains are relatively homogeneous and lower in the grain-boundary with respect to those presented in the coarsest mean grain size. For broader dispersions like $\Delta D/D = 6$ (Fig. 8a,b) all grains become gradually plastic whereas, a proportion of grains and their grain-boundary remain elastic and never reach their own plastic flow stress.

Table 1
Model's parameters for the two phases

Phase	E (MPa)	ν	τ_∞	k_0	a_0	n_{gb}	σ_Y	h_{gb}
Grain	65,900	0.35	105	468	−23.13			
GB	65,800	0.35				0.4	137	10000

Table 2
Hardening parameters for the grain phase

Phase	h_{exp}	h_{ratio}	h_{final}	q
Grain	150	11	103	1.01

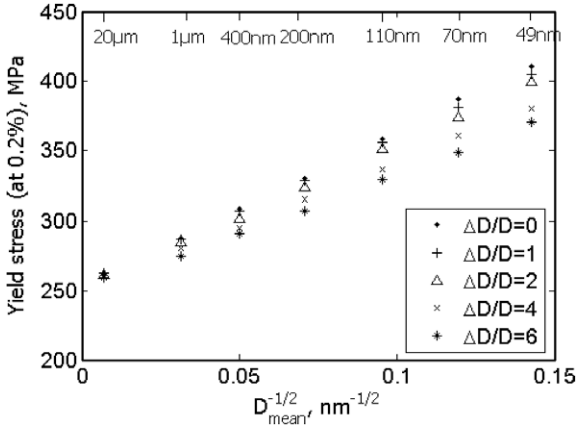

Fig. 4. Predicted yield stress at 0.2% plastic strain as a function of mean grain size for different "relative" dispersions $\Delta D/D$ (D being the mean grain diameter) ranging from 0 to 6.

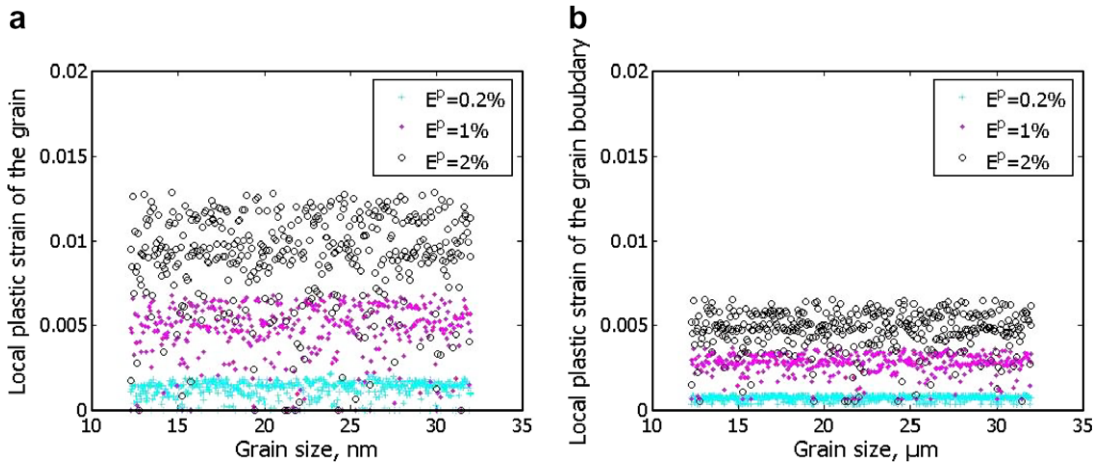

Fig. 5. Local plastic strain distribution vs. grain-size distribution at mean grain size D_{mean} = 20 μm and relative dispersion $\Delta D/D$ = 1 for both grain (a) and grain boundary (b) at three overall axial plastic strains levels E^p = 0.2%, 1.0% and 5.0%.

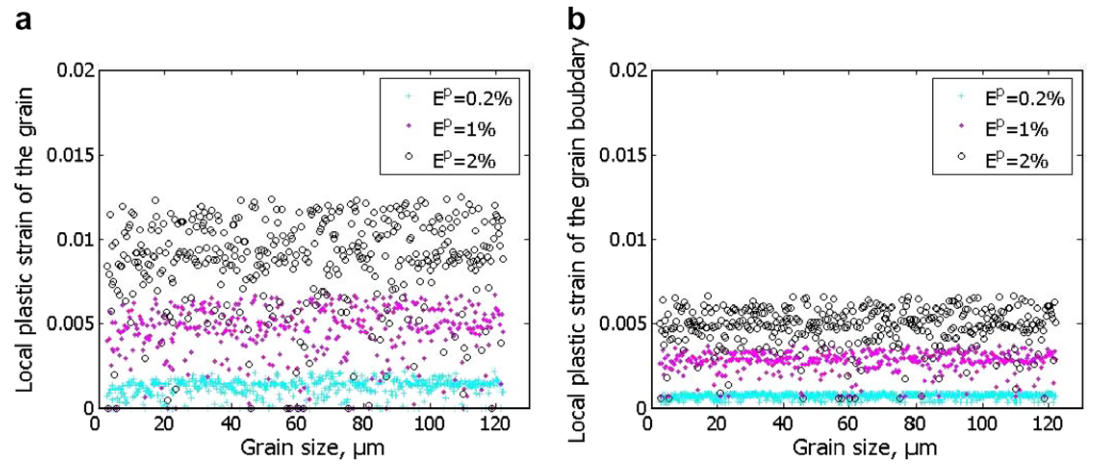

Fig. 6. Local plastic strain distribution vs. grain-size distribution at mean grain size D_{mean} = 20 μm and relative dispersion $\Delta D/D$ = 6 for both grain (a) and grain boundary (b) at three overall axial plastic strains levels E^p = 0.2%, 1.0% and 5.0%.

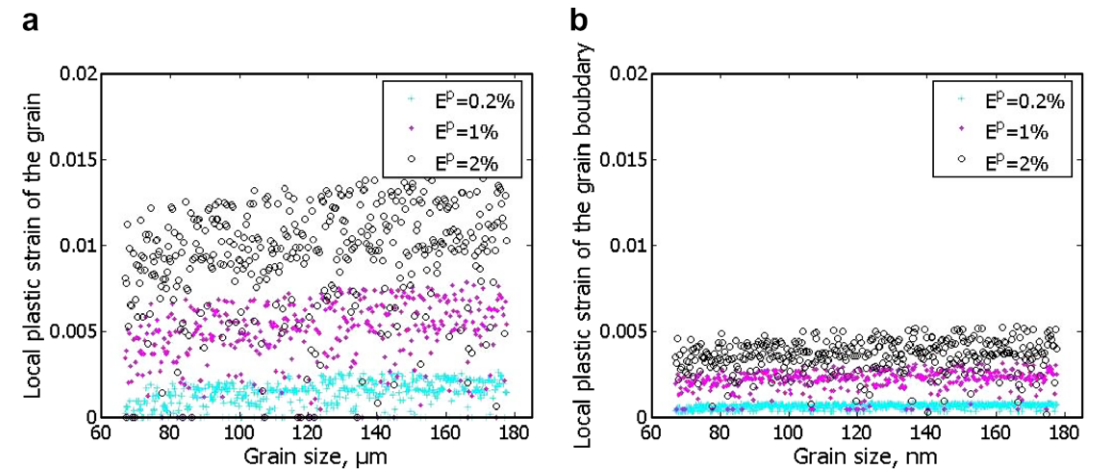

Fig. 7. Local plastic strain distribution vs. grain-size distribution at mean grain size D_{mean} = 110 nm and relative dispersion $\Delta D/D$ = 1 for both grain (a) and grain boundary (b) at three overall axial plastic strains levels E^p = 0.2%, 1.0% and 5.0%.

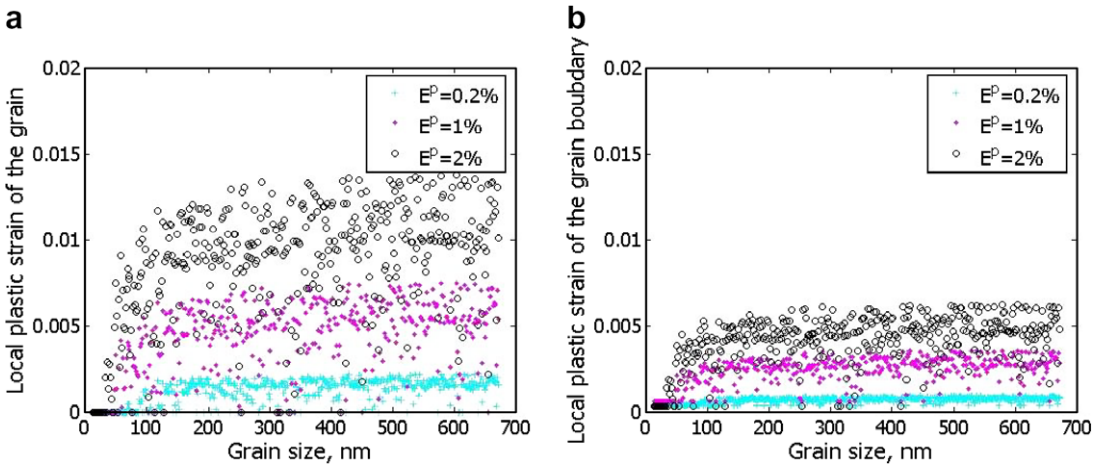

Fig. 8. Local plastic strain distribution vs. grain-size distribution at mean grain size D_{mean} = 110 nm and relative dispersion $\Delta D/D$ = 6 for both grain (a) and grain boundary (b) at three overall axial plastic strains levels E^P = 0.2%, 1.0% and 5.0%.

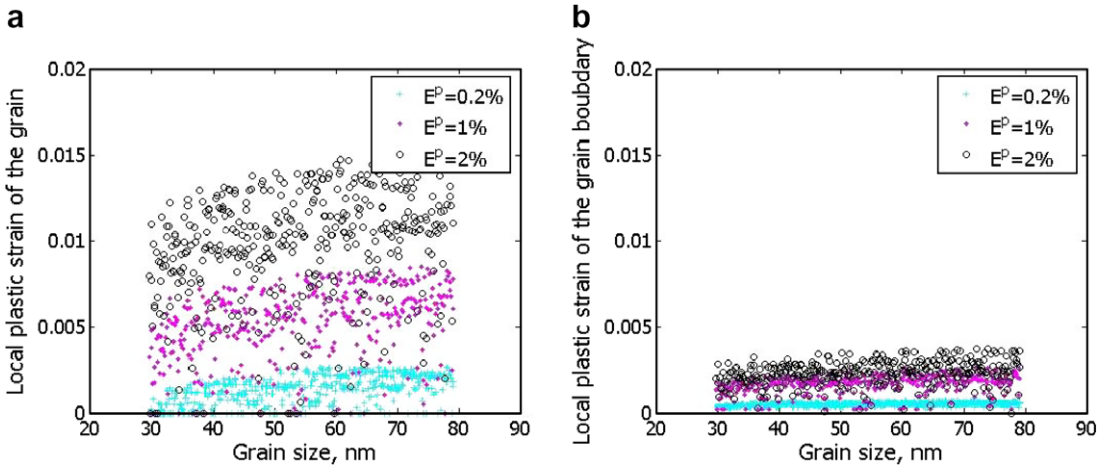

Fig. 9. Local plastic strain distribution vs. grain-size distribution at mean grain size D_{mean} = 49 nm and relative dispersion $\Delta D/D$ = 1 for both grain (a) and grain boundary (b) at three overall axial plastic strains levels E^P = 0.2%, 1.0% and 5.0%.

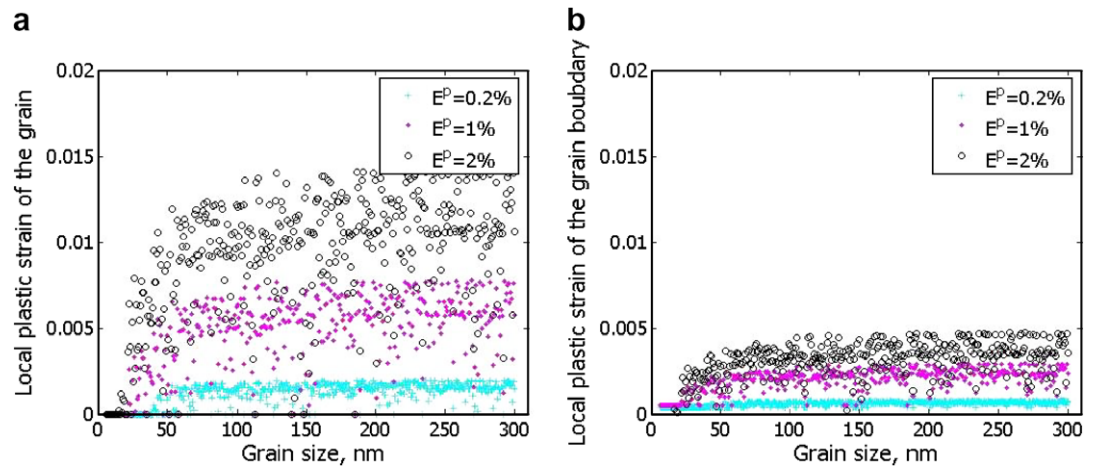

Fig. 10. Local plastic strain distribution vs. grain-size distribution at mean grain size D_{mean} = 49 nm and relative dispersion $\Delta D/D$ = 6 for both grain (a) and grain boundary (b) at three overall axial plastic strains levels E^P = 0.2%, 1.0% and 5.0%.

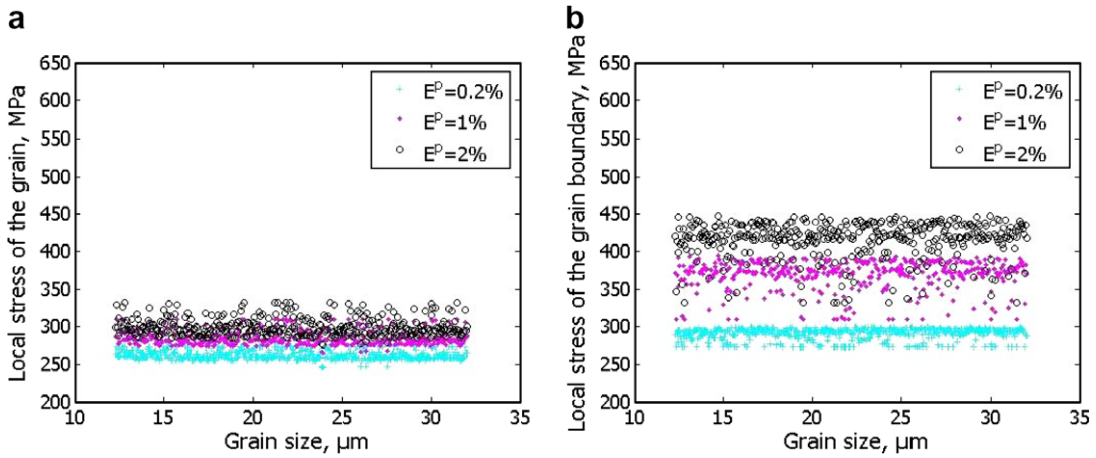

Fig. 11. Local stress distribution vs. grain-size distribution at mean grain size D_{mean} = 20 μm and relative dispersion $\Delta D/D$ = 1 for both grain (a) and grain boundary (b) at three overall axial plastic strains levels E^P = 0.2%, 1.0% and 5.0%.

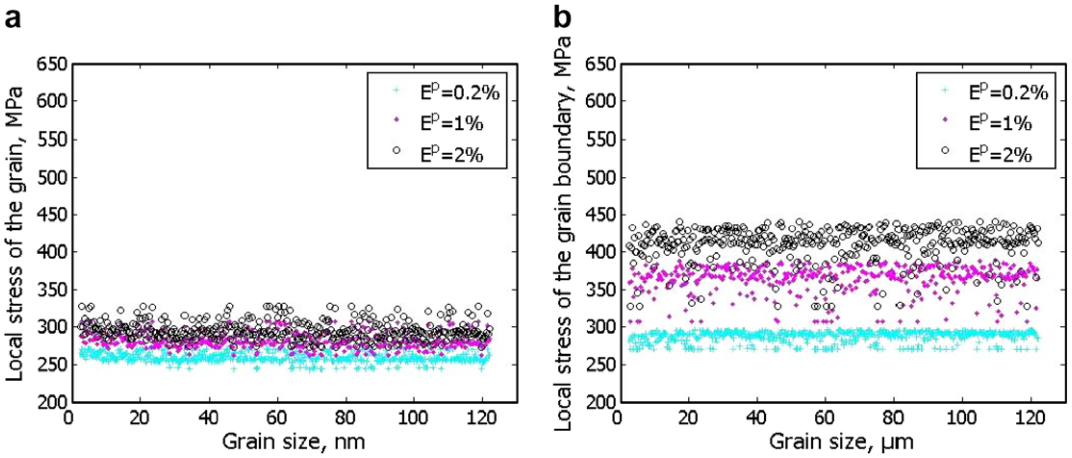

Fig. 12. Local stress distribution vs. grain-size distribution at mean grain size D_{mean} = 20 μm and relative dispersion $\Delta D/D$ = 6 for both grain (a) and grain boundary (b) at three overall axial plastic strains levels E^P = 0.2%, 1.0% and 5.0%.

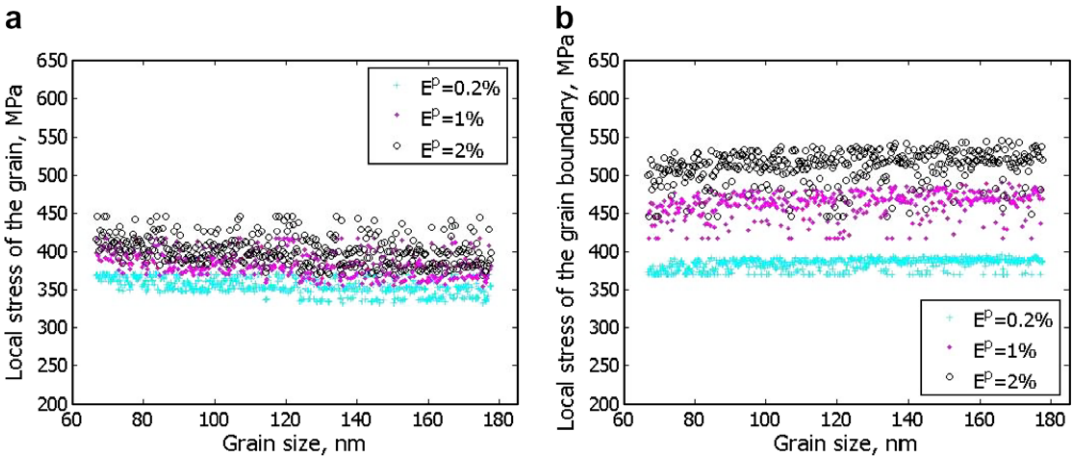

Fig. 13. Local stress distribution vs. grain-size distribution at mean grain size D_{mean} = 110 nm and relative dispersion $\Delta D/D$ = 1 for both grain (a) and grain boundary (b) at three overall axial plastic strains levels E^P = 0.2%, 1.0% and 5.0%.

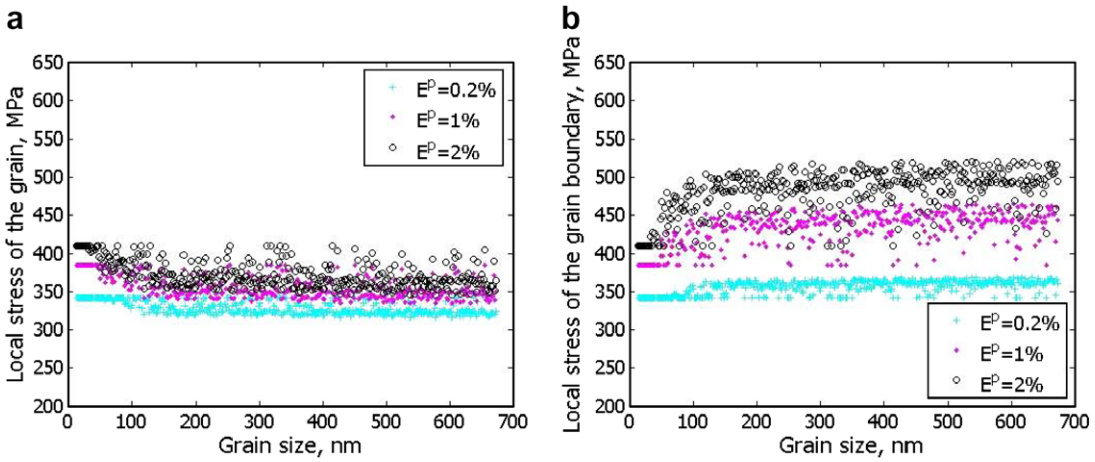

Fig. 14. Local stress distribution vs. grain-size distribution at mean grain size D_{mean} = 110 nm and relative dispersion $\Delta D/D$ = 6 for both grain (a) and grain boundary (b) at three overall axial plastic strains levels E^p = 0.2%, 1.0% and 5.0%.

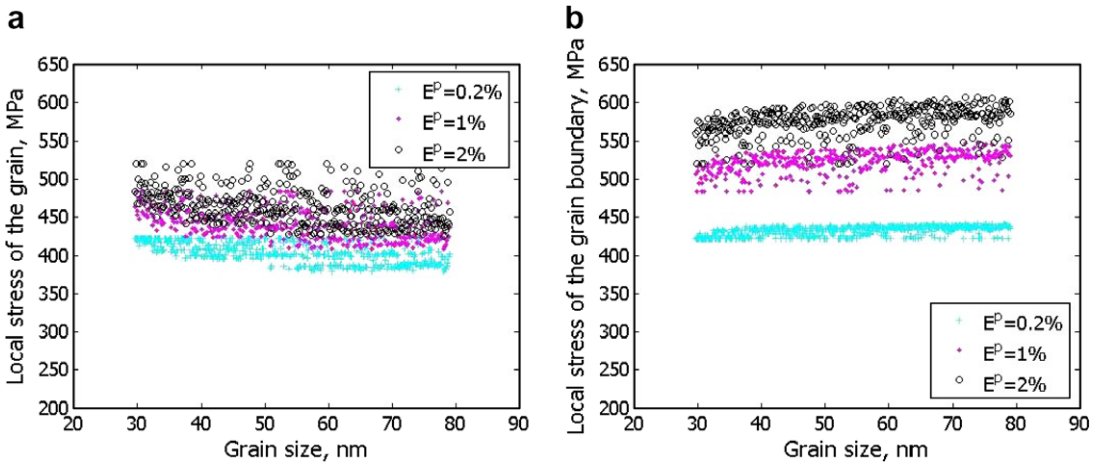

Fig. 15. Local stress distribution vs. grain-size distribution at mean grain size D_{mean} = 49 nm and relative dispersion $\Delta D/D$ = 1 for both grain (a) and grain boundary (b) at three overall axial plastic strains levels E^p = 0.2%, 1.0% and 5.0%.

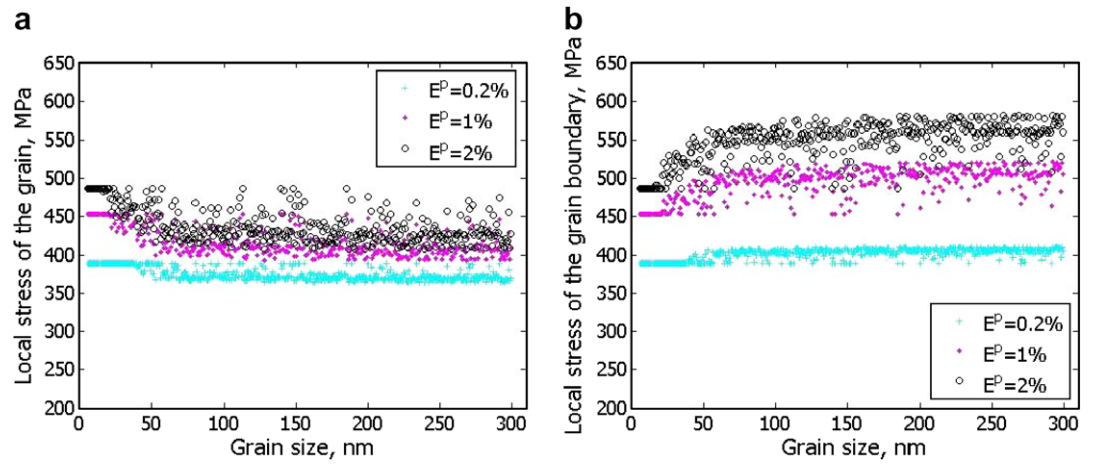

Fig. 16. Local stress distribution vs. grain-size distribution at mean grain size D_{mean} = 49 nm and relative dispersion $\Delta D/D$ = 6 for both grain (a) and grain boundary (b) at three overall axial plastic strains levels E^p = 0.2%, and 5.0%.

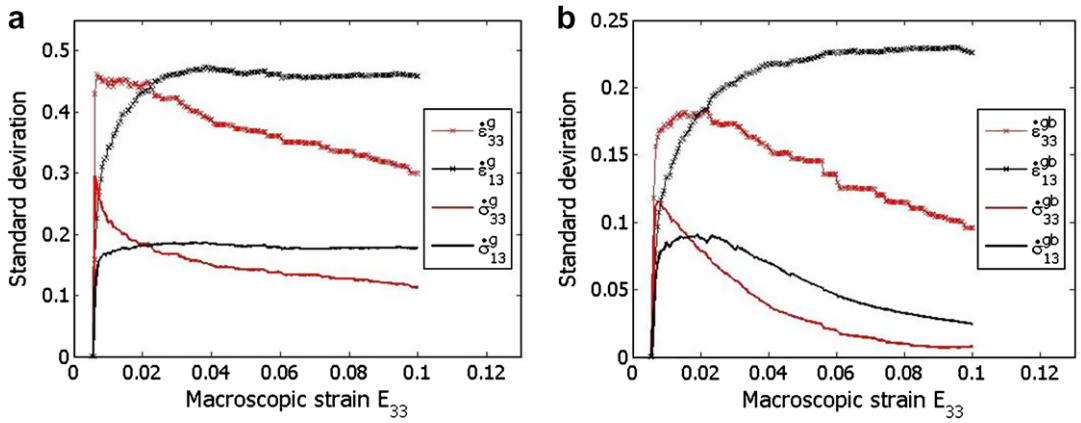

Fig. 17. Standard deviation of normal and shear stress rate and strain rate of grain (a) and of grain boundary (b) as a function the macroscopic train. The calculation for D_{mean} = 49 nm with the relative dispersion $\Delta D/D$ = 0.

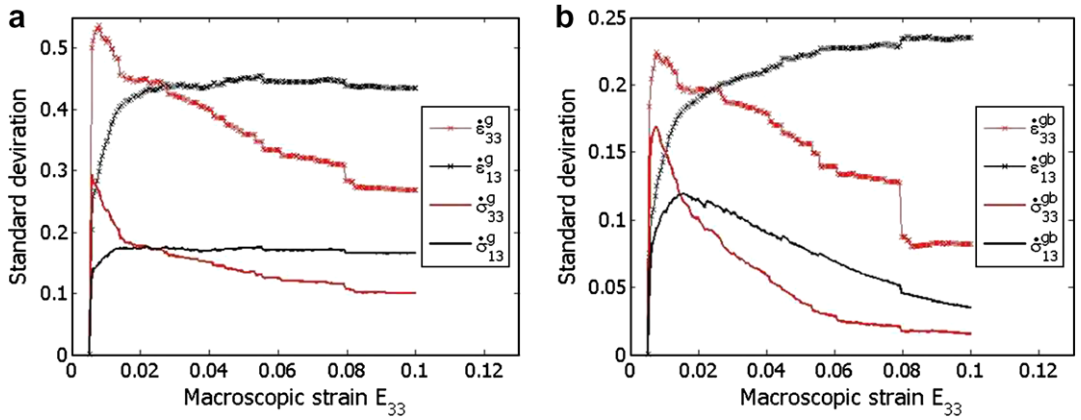

Fig. 18. Standard deviation of normal and shear stress rate and strain rate of grain (a) and of grain boundary (b) as a function the macroscopic train. The calculation for D_{mean} = 49 nm with the relative dispersion $\Delta D/D$ = 6.

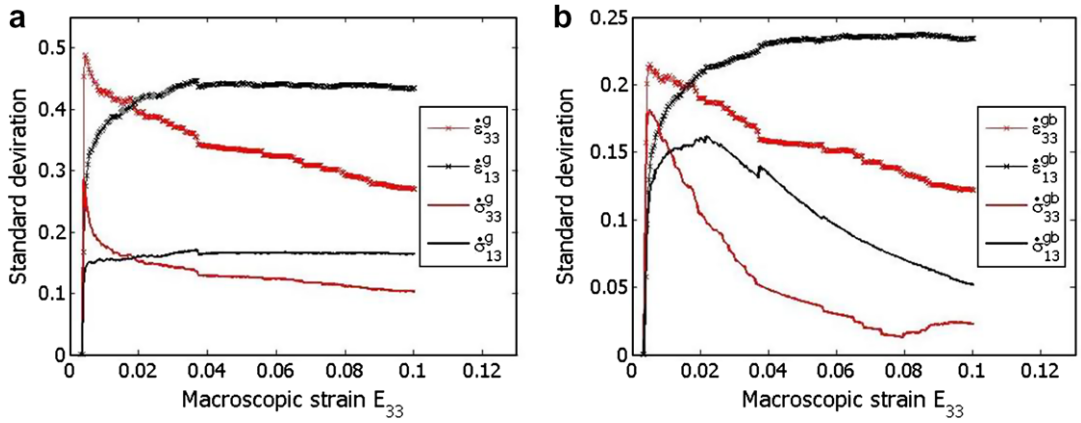

Fig. 19. Standard deviation of normal and shear stress rate and strain rate of grain (a) and of grain boundary (b) as a function the macroscopic train. The calculation for D_{mean} = 20 μm with the relative dispersion $\Delta D/D$ = 0.

Regarding now the mean grain size D_{mean} = 49 nm, it is found that for $\Delta D/D$ = 1, all grains become gradually plastic as in the previous case (Fig. 9a). In the grain boundary (Fig. 9b), the plastic strain distribution is of first order (affine distribution) contrarily to the previous situation which was relatively homogeneous. For broader dispersions like $\Delta D/D$ = 6 (Fig. 10a,b) all grains become gradually plastic whereas, a proportion of grains and their grain-boundary remain also elastic and never reach

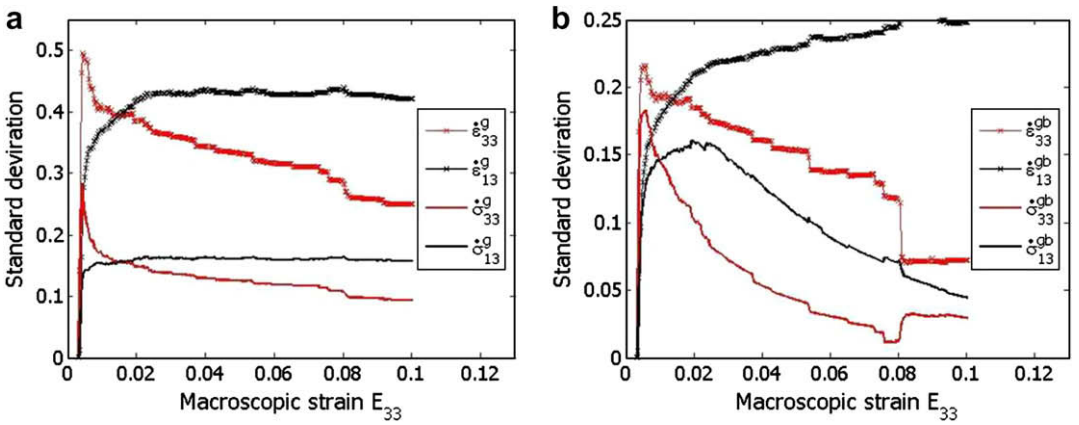

Fig. 20. Standard deviation of normal and shear stress rate and strain rate of grain (a) and of grain boundary (b) as a function the macroscopic train. The calculation for D_{mean} = 20 μm with the relative dispersion $\Delta D/D$ = 6.

their own plastic flow stress. Besides, for $\Delta D/D$ = 6 and D_{mean} = 49 nm, the proportion of grains remaining in an elastic state is sensibly the same than for D_{mean} = 110 nm.

3.3. Internal stress fields

The local stress distribution profiles both in the grains (g) and grain-boundaries (gb) ($\bar{\sigma}_{33}^{(g)}$ and $\bar{\sigma}_{33}^{(gb)}$ in the axial loading direction 3) at three stages of macroscopic tensile plastic strains E_{33}^{p}: 0.2%, 1% and 2% are reported in Figs. 11–16.

The coarsest mean grain size D_{mean} = 20 μm case exhibit homogeneous local stress distribution and which is not affected by the relative dispersion (Figs. 11 and 12). One can note that local stresses are higher in the grain boundary with respect to lowest plastic strain in the same grain-boundary. Now, when analyzing the case of intermediate mean grain size D_{mean} = 110 nm and slight dispersions $\Delta D/D$ = 1 (Fig. 13a,b), the local stress distribution remains quietly homogeneous and highest than in the case of coarsest mean grain size. For broader dispersions like $\Delta D/D$ = 6 (Fig. 14a,b), local stress distribution is decreasing and lower than the overall stress Σ in the grain phase whereas it is increasing and upper than the overall stress Σ in the grain-boundary phase. The same comments can apply for the finest mean grain size D_{mean} = 49 nm (Figs. 15 and 16) with higher levels of local stresses in both phases. It is important to note that for the two last mean grain sizes (i.e. 110 and 49 nm) and broad dispersions like $\Delta D/D$ = 6, the local stress distribution is of second order around the mean grain size before increasing (decreasing for (gb)) linearly while moving away from the mean grain grain-size value.

3.4. Local magnitudes deviation

In order to determine how the local magnitudes deviate with respect to macroscopic magnitudes, Figs. 17–20 shows the comparison between standard deviations (SD) in some stress rates and strain rates components (as a function of macroscopic strain E_{33}). Some general features of these curves are: (a) As elastic isotropy is assumed, all stress and strain are homogeneous up to approximately 0.5%. Heterogeneities start when the easiest slip system in the best oriented grain is activated. (b) The model predicts higher deviations in strain than in stress, keeping close to upper-bound limit. (c) Concerning the grain phase (g), both shear stress and strain are and remain severely heterogeneous (Figs. 17–20a) while the normal strain and stress rates follow a decreasing process with a slope that depends upon the mean grain size and the relative dispersion. (d) About the grain-boundary phase (Figs. 17–20b), it appears that the shear strain rate is extremely heterogeneous while the shear stress rate is decreasing, denoting a homogenization process of this field. Again, the normal strain and stress rates follow a decreasing process, with a slope that depends upon the mean grain size and the relative dispersion, in order to converge to a homogeneous field. In all cases, the SD is higher in the grain phase than in the grain-boundary one.

4. Conclusion

As there is a great need for more understanding the response of heterogeneous materials to external applied loads and especially when the surrounding grain-boundary is investigated with respect to the grain, the authors believe strongly that this work is timely in a way helps provide quantitative insight. Then, a model based on a generalized tangent-self-consistent scheme, and inspired from previous work of Jiang and Weng [22,23], was revisited in order to predict both the mean grain size effect and the lognormal distribution upon the macroscopic behaviour of NC materials. The NC material is modelled as a composite material that takes each oriented grain and its immediate grain boundary to form a pair, which in turn is embedded in the infinite effective medium with a property representing the average orientation of all these pairs. Under small strain assumption, the plastic deformation of the inclusion phase takes into account the dislocation glide mechanism

whereas boundary phase is modelled as an amorphous material. It is clearly shown that characterizing fine grained heterogeneous materials not only by its mean grain size but also in terms of its grain-size distributions should be an important issue to optimize these microstructures and their processing. Then, this model appears to be more relevant than analytical models treating the yield stress as simple mixture rules of components log-normally distributed. For one, not only the mean grain size plays a role but also grain-size dispersion has an impact on the overall yield stress. It is shown that a deviation of the overall yield stress from the local grain size dependent rule occurs. For another, local plastic strains and second order internal stresses which develop within the material have been recorded and discussed depending on the grain-size distribution. It is found that an increase of grain-size dispersion leads to rise plastic heterogeneities within the material around the mean grain size. Local plastic strain and stress fluctuations are even more pronounced for fine-grained materials.

It is well established here, as in previous works [43,44], that the impact of the grain-size distribution is more important for fine-grained materials than for coarse-grained materials.

However, some limitations of the present contribution must be pointed out following some considerations that are particularly important for applications involving finite deformation because the mathematical structure is then more sophisticated and expresses so much more of the essence of the phenomenon [70]. In extending this work to plasticity at large deformation transformation, it is not possible to write a constitutive equation of the form (Eq. 1) involving the rate of Cauchy stress and any "strain rate" since it would not be frame indifferent. On the other hand, if a suitable objective rate is used, the analogy with linear elasticity is completely lost since the objective rate is not divergence free, nor does the linear transformation relating the "stress rate" to the "strain rate" satisfy the symmetry requirements necessary for the establishment of the analogy. Furthermore the processes that create NC materials such as SPD, except perhaps ECAE, and others induce quite a bit of internal stresses in the material [71], which cannot be relieved by annealing without destroying the fine grain size. These initial stresses also invalidate the analogy since the usual elasticity approaches assume that the matrix and the inclusion are simultaneously stress free.

Appendix

Parameters in Christensen and Lo [53], and Luo and Weng [54] models previously stated by paper (Jiang and Weng [22,23]). In this Appendix we have used tangent moduli instead of secant moduli.

Parameters $\bar{\alpha}_g, \bar{\beta}_g, \bar{\alpha}_{gb}$ and $\bar{\beta}_{gb}$

$$\bar{\alpha}_g = \frac{1}{p}(3\kappa_c^t + 4\mu_c^t)(3\kappa_{gb}^t + 4\mu_{gb}^t)\frac{\kappa_g}{\kappa_c^t}$$
$$\bar{\beta}_g = 2\mu_g\left[\bar{a}_1 - \frac{21}{5(1-2\nu_g)}\bar{a}_2\right]$$
$$\bar{\alpha}_{gb} = \frac{1}{p}(3\kappa_c^t + 4\mu_c^t)\left(3\kappa_g + 4\mu_{gb}^t\right)\frac{\kappa_{gb}^t}{\kappa_c^t}$$
$$\bar{\beta}_{gb} = 2\mu_{gb}^t\left[\bar{b}_1 - \frac{21}{5(1-2\nu_{gb}^t)}\frac{1-c_g^{5/3}}{1-c}\bar{b}_2\right].$$

Parameters $\bar{\alpha}_g, \bar{\beta}_g, \bar{\alpha}_{gb}$ and $\bar{\beta}_{gb}$

$$\tilde{\alpha}_g = \frac{3\kappa_g}{p}\left[\left(3\kappa_{gb}^t + 4\mu_c^t\right) - 4c_g\left(\mu_c^t - \mu_{gb}^t\right)\right]$$
$$\tilde{\beta}_g = \tilde{a}_1 - \frac{21}{5(1-2\nu_g)}\tilde{a}_2$$
$$\tilde{\alpha}_g = -\frac{12c_g\kappa_g}{p}(\mu_c^t - \mu_{gb}^t)$$
$$\tilde{\beta}_{gb} = \tilde{b}_1 - \frac{21}{5(1-2\nu_{gb}^t)}\frac{1-c_g^{5/3}}{1-c}\tilde{b}_2.$$

Parameter p

$$p = (3\kappa_g + 4\mu_{gb}^t)(3\kappa_{gb}^t + 4\mu_c^t) - 12c_g(\kappa_g - \kappa_{gb}^t)(\mu_c^t - \mu_{gb}^t).$$

Parameters $\bar{a}_1, \bar{a}_2, \bar{b}_1$ and $\bar{b}_2$

$$\begin{Bmatrix}\bar{a}_1\\ \bar{a}_2\end{Bmatrix} = [\overline{K}]_{2\times2}^{-1}\left([\overline{F}_1]_{2\times2}\begin{Bmatrix}\bar{d}_3\\ \bar{d}_4\end{Bmatrix} + \frac{1}{2\mu_c^t}\begin{Bmatrix}1\\ 1\end{Bmatrix}\right)$$
$$\begin{Bmatrix}\bar{b}_1\\ \bar{b}_2\\ \bar{b}_3\\ \bar{b}_4\end{Bmatrix} = [\overline{G}]_{4\times4}^{-1}[\overline{H}]_{4\times2}\begin{Bmatrix}\bar{a}_1\\ \bar{a}_2\end{Bmatrix},$$

where

$$\begin{Bmatrix} \bar{d}_3 \\ \bar{d}_4 \end{Bmatrix} = [\overline{P}]^{-1}_{2\times2}\left(\frac{1}{2\mu^t_{gb}}\begin{Bmatrix}1\\1\end{Bmatrix} - \frac{1}{2\mu^t_c}[\overline{K}_2]_{2\times2}[\overline{K}_1]^{-1}_{2\times2}\begin{Bmatrix}1\\1\end{Bmatrix}\right)$$

$$[\overline{P}]_{2\times2} = [\overline{K}_2]_{2\times2}[\overline{K}_1]^{-1}_{2\times2}[\overline{F}_1]^{-}_{2\times2}[\overline{F}_2]_{2\times2}$$

$$[\overline{K}_1]_{2\times2} = [\overline{E}_1]_{2\times4}[\overline{G}]^{-1}_{4\times4}[\overline{H}]_{4\times2}$$

$$[\overline{K}_2]_{2\times2} = [\overline{E}_2]_{2\times4}[\overline{G}]^{-1}_{4\times4}[\overline{H}]_{4\times2}$$

$$[\overline{E}_1]_{2x4} = \begin{bmatrix} 1 & -\frac{6\nu^t_{gb}}{1-2\nu^t_{gb}} & 3 & -\frac{5-4\nu^t_{gb}}{1-2\nu^t_{gb}} \\ 1 & -\frac{7-4\nu^t_{gb}}{1-2\nu^t_{gb}} & -2 & 2 \end{bmatrix}$$

$$[\overline{E}_2]_{2x4} = \begin{bmatrix} 1 & \frac{3\nu^t_{gb}}{1-2\nu^t_{gb}} & -12 & -\frac{2(5-\nu^t_{gb})}{1-2\nu^t_{gb}} \\ 1 & -\frac{7+2\nu^t_{gb}}{1-2\nu^t_{gb}} & 8 & \frac{2(1+\nu^t_{gb})}{1-2\nu^t_{gb}} \end{bmatrix}$$

$$[\overline{F}_1]_{2x2} = \begin{bmatrix} 3 & \frac{5-4\nu^t_c}{1-2\nu^t_c} \\ -2 & 2 \end{bmatrix}$$

$$[\overline{F}_2]_{2x2} = \begin{bmatrix} -12 & \frac{2(5-\nu^t_c)}{1-2\nu^t_c} \\ 8 & \frac{2(1+\nu^t_c)}{1-2\nu^t_c} \end{bmatrix}\frac{\mu^t_c}{\mu^t_{gb}}$$

$$[\overline{G}]_{4x4} = \begin{bmatrix} 1 & -\frac{6\nu^t_{gb}c^{2/3}_g}{1-2\nu^t_{gb}} & \frac{3}{c^{5/3}_g} & \frac{5-4\nu^t_{gb}}{(1-2\nu^t_{gb})c_g} \\ 1 & -\frac{(7-4\nu^t_{gb})c^{2/3}_g}{1-2\nu^t_{gb}} & -\frac{2}{c^{5/3}_g} & \frac{2}{c_g} \\ 1 & \frac{3\nu^t_{gb}c^{2/3}_g}{1-2\nu^t_{gb}} & -\frac{12}{c^{5/3}_g} & -\frac{2(5-\nu^t_{gb})}{(1-2\nu^t_{gb})c_g} \\ 1 & -\frac{(7+2\nu^t_{gb})c^{2/3}_g}{1-2\nu^t_{gb}} & \frac{8}{c^{5/3}_g} & \frac{2(1+\nu^t_{gb})}{(1-2\nu^t_{gb})c_g} \end{bmatrix}$$

$$[\overline{H}]_{4x2} = \begin{bmatrix} 1 & -\frac{6\nu_g}{1-2\nu_g} \\ 1 & -\frac{7-4\nu_g}{1-2\nu_g} \\ \frac{\mu_g}{\mu^t_{gb}} & \frac{3\nu_g}{1-2\nu_g}\frac{\mu_g}{\mu^t_{gb}} \\ \frac{\mu_g}{\mu^t_{gb}} & -\frac{7+2\nu_g}{1-2\nu_g}\frac{\mu_g}{\mu^t_{gb}} \end{bmatrix}.$$

Parameters $\tilde{a}_1, \tilde{a}_2, \tilde{b}_1$ and $\tilde{b}_2$

$$\begin{Bmatrix} \tilde{a}_1 \\ \tilde{a}_2 \end{Bmatrix} = [\widetilde{R}]^{-1}_{2\times2}\begin{Bmatrix}1\\1\end{Bmatrix}$$

$$\begin{Bmatrix} \tilde{b}_1 \\ \tilde{b}_2 \\ \tilde{b}_3 \\ \tilde{b}_4 \end{Bmatrix} = [\widetilde{E}]^{-1}_{4\times4}[\widetilde{F}]_{4\times2}[\widetilde{K}]^{-1}_{2\times2}[\widetilde{H}]_{4\times2}[\widetilde{R}]^{-1}_{2\times2}\begin{Bmatrix}1\\1\end{Bmatrix}$$

$$[\widetilde{E}]_{4x4} = \begin{bmatrix} 1 & -\frac{6\nu^t_{gb}}{1-2\nu^t_{gb}} & 3 & \frac{5-4\nu^t_{gb}}{1-2\nu^t_{gb}} \\ 1 & -\frac{7-4\nu^t_{gb}}{1-2\nu^t_{gb}} & -2 & 2 \\ 1 & \frac{3\nu^t_{gb}}{1-2\nu^t_{gb}} & -12 & -\frac{2(5-\nu^t_{gb})}{(1-2\nu^t_{gb})} \\ 1 & -\frac{(7+2\nu^t_{gb})}{1-2\nu^t_{gb}} & 8 & \frac{2(1+\nu^t_{gb})}{1-2\nu^t_{gb}} \end{bmatrix}$$

$$[\widetilde{F}]_{4x2} = \begin{bmatrix} 3 & \frac{5-4\nu^t_c}{1-2\nu^s_c} \\ -2 & 2 \\ -\frac{12\mu^t_c}{\mu^t_{gb}} & -\frac{2(5-\nu^t_c)}{1-2\nu^t_c}\frac{\mu^t_c}{\mu^t_{gb}} \\ \frac{8\mu^t_c}{\mu^t_{gb}} & \frac{2(1+\nu^t_c)}{1-2\nu^t_c}\frac{\mu^t_c}{\mu^t_{gb}} \end{bmatrix}$$

$$[\widetilde{G}]_{2x4} = \begin{bmatrix} 1 & -\frac{6\nu^t_{gb}c_g^{2/3}}{1-2\nu^t_{gb}} & \frac{3}{c_g^{2/3}} & \frac{5-4\nu^t_{gb}}{(1-2\nu^t_{gb})c_g} \\ 1 & -\frac{(7-4\nu^t_{gb})c_g^{2/3}}{1-2\nu^t_{gb}} & -\frac{2}{c_g^{2/3}} & \frac{2}{c_g} \end{bmatrix}$$

$$[\widetilde{H}]_{2x2} = \begin{bmatrix} 1 & -\frac{6\nu_g}{1-2\nu_g} \\ 1 & -\frac{7-4\nu_g}{1-2\nu_g} \end{bmatrix}$$

$$[\widetilde{P}]_{2x2} = \begin{bmatrix} 1 & \frac{3\nu_g}{1-2\nu_g} \\ 1 & -\frac{7+2\nu_g}{1-2\nu_g} \end{bmatrix}$$

$$[\widetilde{G}]_{2x4} = \frac{\mu^t_{gb}}{\mu_g} \begin{bmatrix} -1 & -\frac{3\nu^t_{gb}c_g^{2/3}}{1-2\nu^t_{gb}} & \frac{12}{c_g^{5/3}} & \frac{2(5-\nu^t_{gb})}{(1-2\nu^t_{gb})c_g} \\ -1 & -\frac{(7+2\nu^t_{gb})c_g^{2/3}}{1-2\nu^t_{gb}} & -\frac{8}{c_g^{5/3}} & -\frac{2(1+\nu^t_{gb})}{1-2\nu^t_{gb}c_g} \end{bmatrix}$$

$$[\widetilde{K}]_{2\times2} = [\widetilde{G}]_{2\times4}[\widetilde{E}]^{-1}_{4\times4}[\widetilde{F}]_{4\times2}$$

$$[\widetilde{R}]_{2\times2} = [\widetilde{P}]_{2\times2} + [\widetilde{Q}]_{2\times4}[\widetilde{E}]^{-1}_{4\times4}[\widetilde{F}]_{4\times2}[\widetilde{K}]^{-1}_{2\times2}[\widetilde{H}]_{2\times2}.$$

References

[1] S. Billard, J. Fondere, B. Bacroix, et al, Macroscopic and microscopic aspects of the deformation and fracture mechanisms of ultrafine-grained aluminum processed by hot isostatic pressing, Acta Materialia 54 (2006) 411–421.
[2] P.G. Sanders, J.A. Eastman, J.R. Weertman, Elastic and tensile behaviour of Nanocrystalline copper and palladium, Acta Materialia 45 (1997) 4019–4025.
[3] M. Legros, B.R. Elliott, M.N. Rittner, J.R. Weertman, K.J. Hemker, Philosophical Magazine A 80 (4) (2000) 1017–1026.
[4] C.J. Youngdahl, P.G. Sanders, J.A. Eastman, J.R. Weertman, Compressive yield strengths of nanocrystalline Cu and Pd, Scripta Materialia 37 (1997) 809–813.
[5] H. Gleiter, Nanocrystalline materials, Progress in Materials Science 33 (1989) 223–315.
[6] U. Erb, Electrodeposited nanocrystals: synthesis, properties and industrial applications, Nanostructured Materials 6 (1995) 533–538.
[7] H. Hahn, P. Mondal, K.A. Padmanabhan, Plastic deformation of Nanocrystalline materials, Nanostructured Materials 9 (1997) 603–606.
[8] I.V. Alexandrov, Multiscale studies and modeling of SPD materials, Materials Science and Engineering A 387-389 (2004) 772–776.
[9] H. Gleiter, Nanostructured materials: basic concepts and microstructure, Acta Materialia 48 (2000) 1–29.
[10] W.Q. Cao, G.F. Dirras, M. Benyoucef, B. Bacroix, Room temperature deformation mechanisms in ultrafine-grained materials processed by hot isostatic pressing, Materials Science and Engineering: A 462 (2007) 100–105.
[11] H. Conrad, J. Narayan, On the grain size softening in Nanocrystalline materials, Scripta Materialia 42 (2000) 1025–1030.
[12] R.B. Godiksen, Z.T. Trautt, M. Upmanyu, et al, Simulations of boundary migration during recrystallization using molecular dynamics, Acta Materialia 55 (2007) 6383–6391.
[13] M. Dao, L. Lu, R.J. Asaro, J.T.M. De Hosson, E. Ma, Toward a quantitative understanding of mechanical behaviour of nanocrystalline metals, Acta Materialia 55 (2007) 4041–4065.
[14] M.A. Tschoppa, D.L. McDowell, Grain boundary dislocation sources in nanocrystalline copper, Scripta Materialia 58 (2008) 299–302.
[15] D. Stewart, K.-S. Cheong, Molecular dynamics simulations of dislocations and nanocrystals, Current Applied Physics 8 (2008) 494–497.
[16] J. Schiotz, Atomic-scale modeling of plastic deformation of nanocrystalline copper, Scripta Materialia 51 (2004) 837–841.
[17] N.P. Bailey, J. Schiotz, K.W. Jacobsen, Atomistic simulations of Mg–Cu metallic glasses: mechanical properties, Materials Science and Engineering A 387–389 (2004) 996–1000.
[18] D.J. Benson, H.H. Fu, M.A. Meyers, On the effect of grain size on yield stress: extension into nanocrystalline domain, Materials Science and Engineering A 319-321 (2001) 854–861.
[19] M. Cherkaoui, Q.P. Sun, G.P. Song, Micromechanics modeling of composite with ductile matrix and shape memory alloy reinforcement, International Journal of Solids and Structures 37 (2000) 1577–1594.
[20] H.S. Kim, Y. Estrin, M.B. Bush, Plastic deformation behavior of fine-grained materials, Acta Materialia 48 (2000) 493–504.
[21] L. Capolungo, C. Jochum, M. Cherkaoui, J. Qu, Homogenization method for strength and inelastic behavior of nanocrystalline materials, International Journal of Plasticity 21 (2005) 67–82.
[22] B. Jiang, G.J. Weng, A generalized self-consistent polycrystal model for the yield strength of Nanocrystalline materials, Journal of the Mechanics and Physics of Solids 52 (2004) 1125–1149.
[23] B. Jiang, G.J. Weng, A theory of compressive yield strength of nano-grained ceramics, International Journal of Plasticity 20 (2004) 2007–2026.
[24] M.E. Gurtin, L. Anand, Nanocrystalline grain boundaries that slip and separate: a gradient theory that accounts for grain-boundary stress and conditions at a triple-junction, Journal of the Mechanics and Physics of Solids 56 (2008) 184–199.
[25] J.E. Carsley, J. Ning, W.W. Milligan, S.A. Hackney, E.C. Aifantis, A simple mixtures-based model for the grain size dependence of strength in nanophase metals, Nanostructured Materials 5 (1995) 441–448.
[26] N. Wang, Z. Wang, K. Aust, et al, Effect of grain size on mechanical properties of nanocrystalline materials, Acta Metallurgica et Materialia 43 (1995) 519–528.
[27] H.S. Kim, S.I. Hong, S.J. Kim, On the rule of mixtures for predicting the mechanical properties of composites with homogeneously distributed soft and hard particles, Journal of Materials Processing Technology 112 (2001) 109–113.
[28] H.S. Kim, Y. Estrin, Phase mixture modeling of the strain rate dependent mechanical behavior of nanostructured materials, Acta Materialia 53 (2005) 765–772.
[29] L. Capolungo, C. Jochum, M. Cherkaoui, et al, Homogenization method for strength and inelastic behavior of nanocrystalline materials, International Journal of Plasticity 21 (2005) 67–82.
[30] B. Zhu, R.J. Asaro, P. Krysl, R. Bailey, Transition of deformation mechanisms and its connection to grain size distribution in Nanocrystalline metals, Acta Materialia 53 (2005) 4825–4838.
[31] H.H. Fu, D.J. Benson, M.A. Meyers, Analytical and computational description of effect of grain size on yield stress of metals, Acta Materialia 49 (2001) 2567–2582.
[32] H.H. Fu, D.J. Benson, M.A. Meyers, Computational description of nanocrystalline deformation based on crystal plasticity, Acta Materialia 52 (2004) 2567–2582.

[33] Y.J. Wei, L. Anand, Grain-boundary sliding and separation in polycrystalline metals: application to nanocrystalline fcc metals, Journal of the Mechanics and Physics of Solids 52 (2004) 2587–2616.
[34] D. Warner, J. Molinari, A semi-discrete and non-local crystal plasticity model for nanocrystalline metals, Scripta Materialia 54 (2006) 1397–1402.
[35] Y.M. Wang, K. Wang, D. Pan, K. Lu, K.J. Hemker, E. Ma, Microsample tensile testing of nanocrystalline copper, Scripta Materialia 48 (2003) 1581–1586.
[36] K.S. Kumar, S. Suresh, M.F. Chisholm, J.A. Horton, P. Wang, Deformation of electrodeposited nanocrystalline nickel, Acta Materialia 51 (2003) 387–405.
[37] D. Farkas, S. Van Petegem, P.M. Derlet, H. Van Swygenhoven, Dislocation activity and nano-void formation near crack tips in nanocrystalline Ni, Acta Materialia 53 (2005) 3115–3123.
[38] D. Tanguy, M. Razafindrazaka, D. Delafosse, Multiscale simulation of crack tip shielding by a dislocation, Acta Materialia 56 (2008) 2441–2449.
[39] G.J. Weng, A micromechanical theory of grain-size dependence in metal plasticity, Journal of the Mechanics and Physics of Solids 31 (3) (1983) 193–203.
[40] M. Berveiller, A. Zaoui, An extension of the self-consistent scheme to plastically-flowing polycrystals, Journal of the Mechanics and Physics of Solids 26 (1979) 325–344.
[41] A. Acharya, Beaudoin A.J., Grain-size effect in viscoplastic polycrystals at moderate strains, Journal of the Mechanics and Physics of Solids 48 (2000) 2213–2230.
[42] J. Lian, B. Baudelet, AA. Nazarov, Model for the prediction of the mechanical behaviour of nanocrystalline materials, Materials Science and Engineering A 172 (1993) 23–29.
[43] S. Berbenni, V. Favier, M. Berveiller, Micro–macro modelling of the effects of the grain size distribution on the plastic flow stress of heterogeneous materials, Computational Materials Science 39 (2007) 96–105.
[44] S. Berbenni, V. Favier, M. Berveiller, Impact of the grain size distribution on the yield stress of heterogeneous materials, International Journal of Plasticity 23 (2007) 114–142.
[45] B. Zhu, R. Asaro, P. Krysl, et al, Effects of grain size distribution on the mechanical response of nanocrystalline metals: part ii, Acta Materialia 54 (2006) 3307–3320.
[46] M.A. Meyers, K.K. Chawla, Grain size strengthening, in: Mechanical Metallurgy: Principles and Applications, Prentice-Hall, Englewood Cliffs, New Jersey, 1984, pp. 494–514.
[47] D.R.S. Talbot, J.R. Willis, Variational principles for inhomogeneous nonlinear media, IMA Journal of Applied Mathematics 35 (1985) 39–54.
[48] G.P. Tandon, G.J. Weng, A theory of particle-reinforced plasticity, Journal of Applied Mechanics 55 (1988) 126–135.
[49] P. Ponte Castãneda, The efective mechanical properties of nonlinear isotropic composites, Journal of the Mechanics and Physics of Solids 39 (1991) 45–71.
[50] Y.P. Qiu, G.J. Weng, A theory of plasticity for porous materials and particle-reinforced composites, Journal of Applied Mechanics 59 (1992) 261–268.
[51] G.K. Hu, A method of plasticity for general aligned spheroidal void or 3ber-reinforced composites, International Journal of Plasticity 12 (1996) 439–449.
[52] P. Suquet, Overall properties of nonlinear composites: a modi3ed secant moduli theory and its link with Ponte Castãneda's nonlinear variational procedure, Comptes Rendus De L Academie Des Sciences Serie IIb 320 (1995) 563–571.
[53] R.M. Christensen, K.H. Lo, Solutions for effective shear properties in three phase sphere and cylinder models, Journal of the Mechanics and Physics of Solids 27 (1979) 315–330.
[54] H.A. Luo, G.J. Weng, On Eshelby's inclusion problemin a three-phase spherically concentric solid, and a modi3cation of Mori–Tanaka's method, Mechanics of Materials 6 (1987) 347–361.
[55] E.O. Hall, The deformation and aging of mild steel: III. discussion of results, Proceedings of the Physical Society of London B 64 (1951) 747–753.
[56] N.J. Petch, The cleavage strength of polycrystals, Journal of Iron and Steel Institute 174 (1953) 25–28.
[57] B. Clausen, T. LOrentzeni, T. Leffers, Self-consistent modelling of the plastic deformation of f.c.c. polycrystals and its implications for diffraction measurements of internal stresses, Acta Materialia 46 (1998) 3087–3098.
[58] J.W. Hutchinson, Elastic–plastic behavior of polycrystalline metals and composites, Proceedings of the Royal Society of London A 325 (1970) 101–127.
[59] R. Lebensohn, D. Solas, G. Canova, et al, Modelling damage of Al–Zn–Mg alloys, Acta Materialia 44 (1996) 315–325.
[60] D.C. Drucker, Some implication of work hardening and ideal plasticity, Quaterly of Applied Mathematics 7 (1950) 411–418.
[61] P.E. Donovan, A yield criterion for Pd40Ni40P20 metallic glass, Acta Metallurgica 7 (1989) 445–456.
[62] F. Dalla Torre, H. Van Swygenhoven, M. Victoria, Nanocrystalline electrodeposited Ni: microstructure and tensile properties, Acta Materialia 50 (2002) 3957–3970.
[63] H. Azizi-Alizamini, M. Militzer, W.J. Poole, A novel technique for developing bimodal grain size distributions in low carbon steels, Scripta Materialia 57 (2007) 1065–1068.
[64] P. Sanders, C. Youngdahl, J. Weertman, The strength of nanocrystalline metals with and without flaws, Materials Science and Engineering A 234-236 (1997) 77–82.
[65] P. Pilvin, G. Cailletaud, Identifcation and inverse problems related to material behaviour, in: Bui Tanaka et al. (Eds.), Inverse Problems in Engineering Mechanics, Rotterdam, Balkema, 1994, pp. 79–86.
[66] H. Haddadi, S. Bouvier, M. Banu, C. Maier, C. Teodosiu, Towards an accurate description of the anisotropic behaviour of sheet metals under large plastic deformations: modelling, numerical analysis and identification, International Journal of Plasticity 22 (2006) 2226–2271.
[67] A.H. Chokshi, A. Rosen, J. Karch, H. Gleiter, On the validity of the Hall–Petch relationship in Nanocrystalline materials, Scripta Metallurgica 23 (1989) 1679–1684.
[68] J. Schiotz, K.W. Jacobsen, A maximum in the strength of nanocrystalline copper, Science 301 (2003) 1357.
[69] K.J. Kurzydlowski, Scripta Metallurgica Materialia 24 (1990) 879.
[70] J. Gittus, J. Zarka, S. Nemat-Nasser, Large deformation of solids: physical basis and mathematical modelling, Elsevier Applied Science Publishers LTD, 1986.
[71] I.V. Alexandrov, R.Z. Valiev, Developing of SPD processing and enhanced properties in bulk nano structured metals, Scripta Materialia 44 (2001) 1605–1608.